JOTCSA
Journal of the Turkish Chemical Society
Section: A
Chemistry
TURKISH CHEMICAL SOCIETY

Improvement of The CO_2 Sensitivity of HPTS Along With ZnO/CuO Nanoparticles: A Comparative Study Between Core-Shell and Hybrid Structures

Sibel Oğuzlar[1]*
[1]Dokuz Eylul University, Center for Fabrication and Application of Electronic Materials, 35390, Izmir, Turkey

Abstract: Semiconductor metal oxide materials have gained huge attention in gas sensors owing to their high sensitivity to many target gases. Herein, ZnO/CuO core-shell and ZnO/CuO hybrid, which were synthesized by different sol-gel methods and formed in two different crystal structures, were used as an additive material to enhance the response range of 8-hydroxypyrene-1, 3, 6-trisulfonic acid (HPTS) for the sensing of gaseous carbon dioxide. Metal oxide materials were characterized by using XPS, XRD, FTIR, SEM, UV–Vis, and PL spectroscopy. The HPTS dye along with the ZnO/CuO hybrid material displayed a higher CO_2 gas sensitivity as 94% ratio (I_0/I_{100}=16.90) and Stern-Volmer constant (K_{SV}) value and extended linear response range compared to the HPTS-based sensing thin films along with ZnO/CuO core-shell material and additive-free form. ZnO/CuO core-shell and hybrid structures were used for enhancing of carbon dioxide sensitivity of the HPTS dye.

Keywords: Photoluminescence, optical-based carbon dioxide sensor, HPTS, metal oxide, ZnO/CuO core-shell / hybrid.

Submitted: June 02, 2021. **Accepted:** August 23, 2021.

Cite this: Oğuzlar S. Improvement of The CO2 Sensitivity of HPTS Along With ZnO/CuO Nanoparticles: A Comparative Study Between Core-Shell and Hybrid Structures. JOTCSA. 2021;8(4):983–94. .

DOI: https://doi.org/10.18596/jotcsa.947087.

***Corresponding author:** e-mail: sibel.oguzlar@deu.edu.tr.

INTRODUCTION

Detection of carbon dioxide (CO_2) has great significance in various applications like clinical analysis, chemical analysis, and environmental monitoring (1,2). For this reason, it is very critical to measure CO_2 values accurately, continuously, and precisely. The CO_2 can be measured by infrared (IR) spectrometry (3), severinghaus glass electrode (4), and optical sensors (5–7). Recently, the usage of optical-based sensors for the quantitative determination of CO_2 presents many advantages according to other detection methods and reduced noise interference, electrical isolation, remote sensing, and the possibility of miniaturization. The working principle of most optically based carbon dioxide sensors is based on the colorimetric or fluorometric changes of the pH indicators. Reham et al. reported a scheme for sensing CO_2 with a low concentration range by detecting the dual luminescence of the upconverting nanoparticles emission together with bromothymol blue (BTB) (1). A pH-sensitive indicator dye as di-OH-aza-BODIPY was presented by Schutting et al. (8). Schutting and co-workers also introduced new pH indicators based on diketo-pyrrolo-pyrrole (DPP) dye, which becomes highly soluble in polymers and organic solvents with the addition of dialkylsulfonamide groups for optical CO_2 sensors (9).

Borchert and colleagues reported an optochemical CO_2 sensor using a colorimetric pH indicator α-naphthathalene that was included into the plastic matrix together with a phosphorescent reporter dye PtTFPP and a phase transfer agent tetraoctyl- or cetyltrimethylammonium hydroxide (10). Among the used dyes in optical-based CO_2 sensors, the most commonly used pH-sensitive fluorescent dye

has been the trisodium salt of the 1-hydroxy-3, 6, 8 pyrenetrisulfonic acid (HPTS) or ion pair form of HPTS. HPTS has distinct emission and absorption bands in the visible light area (6). Fluorescent HPTS dye, which is pH sensitive, has previously been used in many carbon dioxide sensor studies (11–15). pH-sensitive and fluorescence-based HPTS dye embedded in an organically modified silica (ORMOSIL) glass matrix were utilized for CO_2 gas monitoring (16). Bültzingslöwen et al. presented an optical sol-gel based carbon dioxide sensor with a fast and reversible response in a wide concentration range (0-100% CO_2) based on the luminescent dye HPTS (11). Ertekin et al. presented a new fiber optic detection device using the fluorescence HPTS dye in ion pair form in a capillary reservoir, encapsulated in an ethylcellulose matrix (17).

It can be concluded from these studies that the researchers employed hydrophobic polymers; ethylcellulose, silicon, poly (1-trimethylsilyl-1-propyne), polyethylene, polymethyl methacrylate, and sol-gel as matrix materials with or without additives either in the thin film, composite, micro-nanofiber, and/or micro-nano particle forms. Oter and et al. reported the ionic liquids and perfluorocompounds in the same matrix for more sensitive determination of CO_2 gas with the signal change of bromothymol blue (BTB). They reported that the electrospun nanofibers offered enhanced sensitivity extending to 98% relative signal change (18). By the way, Ongun and et al. presented two novel coordination polymers for usage as sensor additives with HPTS with the result of I_0/I_{100} value as 6.80 and 10.33 for CP1 and CP2, respectively (19). However, further studies for the usage of new matrix materials are still required to enhance the sensitivity and stabilization of the sensors to develop fluorescent optics-based CO_2 sensors, the specific properties of both the sensitive dye and the matrix material need to be viewed and improved.

Semiconducting metal oxides (SMO) are promising candidate materials for gas sensing applications due to their easy production methods, high sensitivity to many target gases, low cost and is highly compatible with other processes (20). Nanomaterials are already established in the field of gas detection due to their high sensitivity, especially due to their large surface/volume ratio. Recently, many heterojunctions containing ZnO and other metal oxides have become a new and popular application to improve electronic tape structure and improve gas detection performance. For example, studies have been conducted on ZnO/TiO_2, NiO/ZnO, CuO/NiO/ZnO, $ZnFe_2O_4$/ZnO, CuO/ZnO structures (21).

The use of CuO and ZnO materials together among the related metal oxides can increase the change of conductivity, thus increasing the gas sensitivity of the materials. However, it has been shown in the studies that the formation of p-CuO/n-ZnO heterostructures increases the gas detection performance (22). Zhyrovetsky et al. reported optical-based gas detection properties of several metal oxide nanoparticles like ZnO, ZnO:Cu, ZnO:Sn, ZnO:Au, ZnO:Ni, TiO_2, SnO_2, ZnO:Pt, WO_3 in several gas environments such as O_2, N_2, H_2, CO, CO_2 (23). The sensor based on the p-CuO/n-ZnO heterojunction fabricated by Ramachandran and co-workers exhibited the enhancement for gas-sensing performance to the ethanol (24). Wang et al. presented that CuO/ZnO composite nanostructure has more CO gas detection capability than single phase ZnO nanowires (25). According to the literature, many gas sensor studies containing metal oxide are based on electrical measurement. The advantage of the luminescence-based measurement used as an alternative in the absence of electrical contact between the resulting impurities and nanostructures. In addition, real-time information about the variation of certain additives in the photoluminescence spectra can be observed. However, the effect of adsorbed gases on the photoluminescence of metal oxide powders has not yet been adequately studied.

In this study, the CuO/ZnO hybrid and CuO/ZnO core-shell particles have been synthesized by the complex-directed hybridization and sol-gel approaches, respectively, and were characterized as morphological, structural, and optical properties. As far as we know, the CuO/ZnO particle additives were previously not used for the enhancement of carbon dioxide sensitivity of the HPTS ion pair dye. The aim of this study is to improve the emission-based response of HPTS dye to CO_2 gas with the synthesized metal oxide additive in our laboratories. Herein, the carbon dioxide-induced emission response of the highly sensitive dye-doped thin film in the PMMA matrix was measured along with a range of different CO_2 concentrations. Upon exposure to different concentrations of CO_2, the sensitivity values of I_0/I_{100} were 10.16 and 16.90 for core-shell ZnO/CuO and hybrid ZnO/CuO immobilized PMMA thin films, respectively.

EXPERIMENTAL SECTION

Reagents

All utilized chemicals were of analytical purity. The CO_2 sensitive and pH indicator fluorescent dye, 8-hydroxypyrene-1,3,6-trisulfonic acid trisodium salt (HPTS) was used in the ion pair form as synthesized before (26). The trisodium salt of HPTS and TOABr were mixed as 1:4 ratio in 1% sodium carbonate solution and CH_2Cl_2 (1:1). Based on the formation of the ion pair, the organic and aqueous phases were separated with a separating funnel and the organic solvent was evaporated to obtain the ion pair. The HPTS dye, additive tetrabutylammonium hydroxide (TBAOH) was supplied from Fluka. The ionic liquid 1-butyl-3-methylimidazolium tetrafluoroborate

($BMIMBF_4$), dioctylphthalate (DOP), polymethyl methacrylate (PMMA), and the solvents of ethanol and tetrahydrofuran (analytical grade) were obtained from Sigma. Nitrogen and carbon dioxide gases were 99.9% purity and supplied from Tinsa Gas, Izmir, Turkey. Copper(II) acetate dihydrate ($Cu(CH_3CHOO)_2\times2H_2O$), Zinc acetate dihydrate ($Zn(CH_3COO)_2\times2H_2O$), sodium hydroxide (NaOH), boric acid (H_3BO_3) were supplied from Sigma Aldrich.

Instrumentation

The phase structure of the synthesized powders was investigated by an X-ray diffractometer (XRD, Thermo Scientific ARL X-ray diffractometer, Cu-Kα, 1.5405 Å, 45kV, 44mA). X-ray photoelectron spectroscopy (XPS, Thermo Scientific K-Alpha) with a monochromatic Al-Kα (1486.7 eV) X-ray source and a beam size of 400 μm diameter was studied to determine the elemental composition of metal oxide samples. Functional groups of powders were evaluated by Fourier transform infrared spectroscopy (FTIR, Thermoscientific Nicolet I10). UV-visible diffuse reflectance spectroscopy (UV-vis DRS) measurement was performed to identify absorbance spectra with Thermo Scientific Evolution 600. Microstructure images for morphological characterization were studied with scanning electron microscopy (SEM, COXEM EM-30 Plus) at different magnifications. The steady-state photoluminescence (PL) emission, excitation, and decay time measurements were carried out by FLSP920 Fluorescence Spectrometer, Edinburgh Instruments. The CO_2 and N_2 gases were blended in the 0–100% concentration range by a Sonimix 7000A gas blending system for carbon dioxide detection measurements. Mixtures of gases were introduced into the sensing membrane via a diffuser needle under ambient conditions after the gases were humidified at a constant relative humidity level of 100%. The humidification of the gases was accomplished by bubbling the gas stream through thermostated wash bottles filled with water at 25 °C at a constant relative humidity level of 100%.

Synthesis of ZnO/CuO Particles via Two Methods

The ZnO/CuO hybrid and ZnO/CuO core-shell particle (1:1 ratio) samples were synthesized similarly, as based on the literature (27,28). 0.25 M ($Zn(CH_3COO)_2\times2H_2O$) and 0.25 M ($Cu(CH_3CHOO)_2\times2H_2O$) solutions were stirred with the addition of NaOH pellets to prepare the ZnO/CuO hybrid composites. Upon keeping the final solution 12h at 120 °C, the calcination process applied as 400 °C for 2.5 h. To prepare the ZnO/CuO core-shell structure, 1 M ($Zn(CH_3COO)_2\times2H_2O$) solution was prepared with the addition of NaOH pellets. The obtained final powders with drying at 75 °C for 2h were added into the 0.35 M ($Cu(CH_3CHOO)_2\times2H_2O$) solution. After waiting for 18 h, bluish precipitates were dried at 100 °C for 1 h to obtain core-shell particles. Both of the synthesized particles were characterized and used as additive materials to enhance the response of the HPTS indicator dye for CO_2 gas sensing measurements.

Thin Film Preparation

The PMMA based carbon dioxide sensing thin films were made by stirring 120 mg of PMMA, 96 mg of plasticizer (DOP), 24 mg of $[BMIM][BF_4]$, 2 mg of HPTS ion pair dye, and 10 mL of THF/EtOH (1:1) mixture in presence and absence of additive materials; 5 mg ZnO/CuO hybrid and 5 mg ZnO/CuO core-shell metal oxide particles. Table 1 presents the compositions of the utilized cocktails. The solutions were mixed under magnetic stirring to provide homogeneity. The obtained polymeric cocktail compositions were spread onto a 125 mm MylarTM type polyester support to obtain thin films. The sensing films were cut to 1.2×3.0 cm and placed crosswise in the quartz cuvette and then emission/excitation-based spectra were taken. All sensing composites contain 25% of polymeric matrices $[BMIM]$ $[BF_4]$, optimized in our previous studies (29). The used ionic liquid increased the stability of the sensing slides and carbon dioxide solubility due to their unique properties such as their reversible solubility with gases. This high solubility results from the formation of Lewis acid-base complexes between the CO_2 anion (electron-pair acceptor) and the ionic liquid (electron-pair donor). The ZnO/CuO hybrid nanocomposite and ZnO/CuO core-shell metal oxide samples were encoded as ZCO-HC and ZCO-CS, respectively.

Table 1: Cocktail compositions used as CO_2-sensing agents.

Dye	Coctail Name	PMMA (mg)	THF (mL)	DOP (mg)	TBAOH (μL)	Ionic liquid (mg)	Additive / ZCO-H (mg)	Additive / ZCO-CS (mg)
HPTS (2 mg)	HPTS_Additive free	120	2.00	96	200	24	-	-
	HPTS_ZCO-H	120	2.00	96	200	24	5	-
	HPTS_ZCO-CS	120	2.00	96	200	24	-	5

RESULTS AND DISCUSSION

Characterization of Synthesized Nanoparticles

The structural changes of the produced particles were examined by XRD. Figure 1 (a) shows XRD patterns for both ZCO-H and ZCO-CS particles, respectively. The recorded patterns exhibit all of the major peaks of a monoclinic CuO phase (JCPDS:48-1548) and also a hexagonal wurtzite ZnO phase (JCPDS:36-1451) for both samples (27,28). The variation in peak positions and their corresponding intensities can be attributed to the change of synthesized methods as a hybrid structure and also the core ZnO and CuO shell in the ZnO/CuO.

Additionally, FTIR analysis was carried out to determine the molecular structure of the synthesized particles. Figure 1 (b) indicates the FTIR spectra of both the ZCO-H and ZCO-CS powders. All relevant peaks according to the obtained spectra are shown in Table 2.

Table 2: FTIR spectra data for ZCO-H and ZCO-CSO powders.

Sample	Wavelength/cm^{-1}	Vibration Type
ZCO-H / ZCO-CS	3000 - 3700	O-H stretching vibration modes
	1100 - 1500	C-H bending (symmetrical)
	1500 - 1750	O-H bending vibration modes
	400 - 700	u(M-O) stretching modes

The absorbance spectra (See Fig. 1 (c)) measurements were performed by using UV-Vis DRS. As it is seen from the spectra, both samples exhibit strong absorption with a maximum of around 350 nm in the UV range.

The XPS analysis was studied to clarify the surface chemical structure of all prepared particles in terms of binding energies and atomic weight (%) values of available elements. The binding energy (BE) peaks around 1022 eV for the Zn2p, 934 eV for the Cu2p, 531 eV for the O1s, and 285 eV for the C1s were in evidence for both ZCO-H and ZCO-CS that are presented in Figure 1 (d).

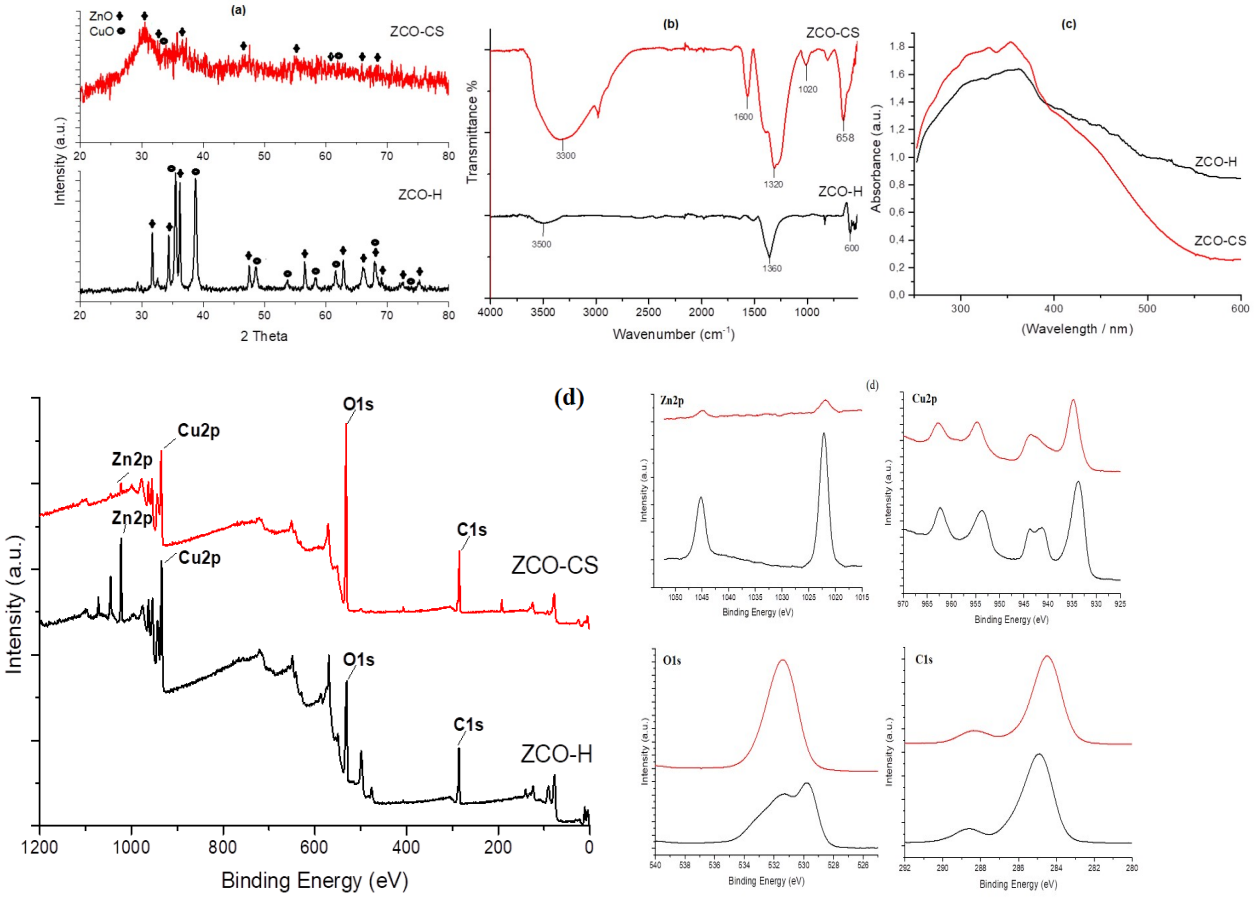

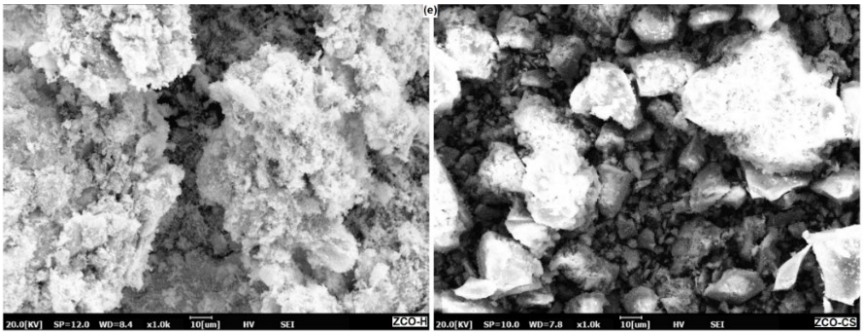

Figure 1: a) XRD patterns, **b)** FTIR spectra, **c)** UV-Vis. Spectra, **d)** XPS spectra, **e)** SEM images of both ZCO-H and ZCO-CSO particles.

According to the information given in the literature, while the binding energy for Cu2p shifts to lower energy than pure CuO, and the binding energy for Zn2p shifts to higher binding energy than pure ZnO upon to the ZnO/CuO structure formation. This binding energy change in XPS measurement is mainly assigned to the difference in electronegativity between the metal ions (30). The fact that the electronegativity value of Cu^{2+} is 2.0 and this value of Zn^{2+} is 1.7 causes the electrons to remove from Zn^{2+} to Cu^{2+}. So the electron-shielding effect of Cu^{2+} is improved and the main peak of Cu2p shifts at lower binding energy, while the main peak of Zn2p shifts to higher binding energy (31). Considering this information, when both materials are examined, the highest shift in both Zn2p and Cu2p values according to binding energies of pure CuO and ZnO (31) was observed for ZCO-H. Meanwhile, the XPS spectra of O 1s can be placed on peaks with the binding energy of 529.78 eV and 531.29 eV for ZCO-H. According to the former studies, the 529.78 eV peak is attributed to the lattice oxygen (O_2^-) on the metal oxide structure, while the 531.29 eV peaks belong to the presence of O^{2-} at the surface. By the way, it has been reported that the sensor sensing performance is due to the adsorbed oxygen on the surface of the material reacting with the target gas (31) (See Table 3).

Table 3: Binding energy (BE) and atomic weight % values according to XPS survey analysis of all samples.

	ZCO-H		ZCO-CS	
Name	**Peak BE**	**Weight %**	**Peak BE**	**Weight %**
Zn2p	1022.15	15.18	1021.88	3.67
Cu2p	933.48	40.05	934.53	36.71
O1s	531.29	25.20	531.18	37.58
C1s	285.87	19.57	285.12	22.04

The SEM micrographs were performed to search for the morphology and microstructure of the hybrid and core/shell particles and the results were shown in Fig. 1 (e). According to the obtained results, the particles are agglomerated. However, some large particles present in the structure and aggregation of nanoparticles can be assigned to the high surface area and surface energy of ZnO particles. In ZnO/CuO particles, the formation of p-n heterojunctions between p-type CuO and n-type ZnO along with pores and voids also contributes to sensitivity. Previous reports presented that the interface between CuO and ZnO plays an important role in gas sensitivity. In our study, ZCO-H material has much finer pores and voids in the structure.

Emission and Excitation Spectra of HPTS and the Utilized Metal Oxide Powders

The excitation and emission spectra of HPTS dye, ZCO-H, and ZCO-CS particles were shown individually in Figure 2.

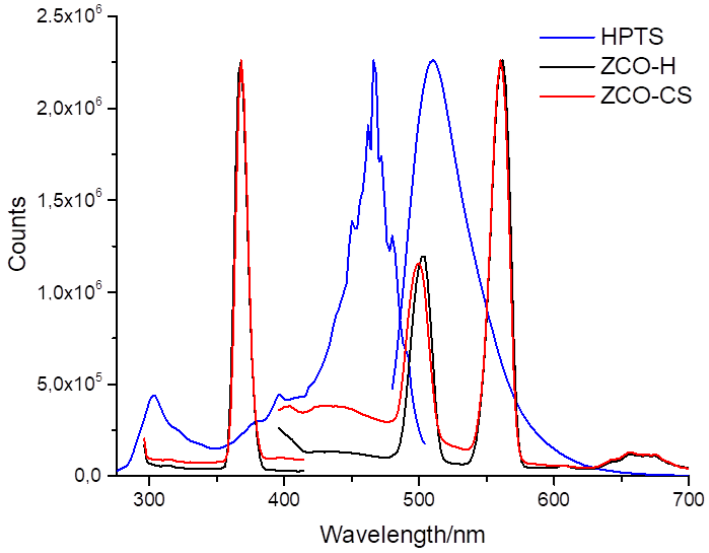

Figure 2: The excitation and emission spectra of the PMMA embedded HPTS, ZCO-H, and ZCO-CS.

In accordance with the literature, HPTS dye exhibited an excitation peak at 380, 405, and 467 nm and also an emission peak at 515 nm when it is embedded in the PMMA matrix (32). The existence of different excitation wavelengths indicates whether the structure is protonated or unprotonated. However, when the dye is exposed to CO_2 gas, the peak at 405 nm increases, whereas the peak at 467 nm decreases with an isobestic point at 419 nm.

The presence of additives significantly increased the CO_2-induced sensitivity of HPTS, increasing the I_0/I_{100} parameter from 6.36 to 10.16 and 16.90 for sensing agent dye along with the ZCO-CS and ZCO-H additives, respectively. So, in this study, we measured the excitation and emission spectra of HPTS dye and the additives of ZCO-H and ZCO-CS heterostructures independently in order to clarify the reasons lying behind the enhancement to CO_2–induced sensitivity (See Fig. 2). Both ZCO-H and ZCO-CS have strongly absorbed between 300 and 420 nm and emitted in a wide range of 400 to 700 nm that covers the excitation band of HPTS. This result enables an energy transfer between the synthesized metal oxide particles and the HPTS dye.

The mechanism underlying the strong emission and absorption capabilities of the ZnO/CuO heterostructure involves bandgap excitation by energetic photons that produce holes in the crystalline valence band and exciton pairs with electrons in the conduction band. Also, the p-n hetero formation plays an important role in improving the detection performance (21,24). However, it can also be attributed to the larger depletion layer on the CuO/ZnO surface, which results from the formation of p-n heterojunctions between the p-CuO and n-type ZnO particles (24).

CO_2 Induced Response of HPTS Based Sensing Slides

Figures 3, 4, and 5 reveal CO_2-induced variations of the excitation and emission spectra of HPTS-based sensing thin films in the absence and the presence of the ZCO-CS and ZCO-H additives, respectively. Intensity-based emission/excitation measurements were performed upon exposure of sensing PMMA-based thin films to 0, 10, 20, 40, 60, 80, and 100% gaseous CO_2 after humidification of the gas.

Herein, the effects of synthesized ZCO-H and ZCO-CS particles on the CO_2 sensitivity of HPTS dye were investigated. It was expected an enhancement in the performance of the dye is expected by the formation of the p-n heterojunction, which reveals a wide depletion region properties of the additives. As a result, HPTS based thin films showed high sensitivity and good linearity in certain concentration ranges along with the additives.

In this study, the Stern-Volmer constant was used for quantitative measurements of photoluminescence-based quenching (Eq. 1):

$$\frac{I_0}{I} = 1 + K_{SV}[CO_2] \qquad \text{(Eq. 1)}$$

where I_0 and I are the emission intensities of without and with a quencher, respectively; $[CO_2]$ is the carbon dioxide concentration, K_{SV} is the collisional quenching constant, called the Stern–Volmer constant. The equation indicates that I_0 / I increases directly proportional to the concentration of the quencher (33).

Figure 3 indicates the CO_2-induced spectral behavior of the additive-free HPTS embedded in PMMA thin

film for the 0-100% [CO_2] concentration range. In the case of excitation at 467 nm, the decrease of the emission intensities was observed at 515 nm. The I_0/I_{100} value which shows the sensitivity of the sensor has been recorded as 6.36 with a linear response, which can be characterized by the equation y = 0.0084x + 1 and R^2 value of 0.9818. However, the I_0/I_{100} values of the sensing films in presence of ZCO-CS and ZCO-H additives were enhanced to 10.16 and 16.90, respectively (see Table 2). This result can be assigned to the absorption and emission abilities of the ZnO/CuO particles as well as the large surface-to-volume ratio and the defects in the ZnO/CuO system (34). All of the HPTS based sensing slides exhibited good carbon dioxide sensitivity (I_0/I_{100}), regression coefficients, and K_{SV} values for the concentration range of 0-100% p[CO_2].

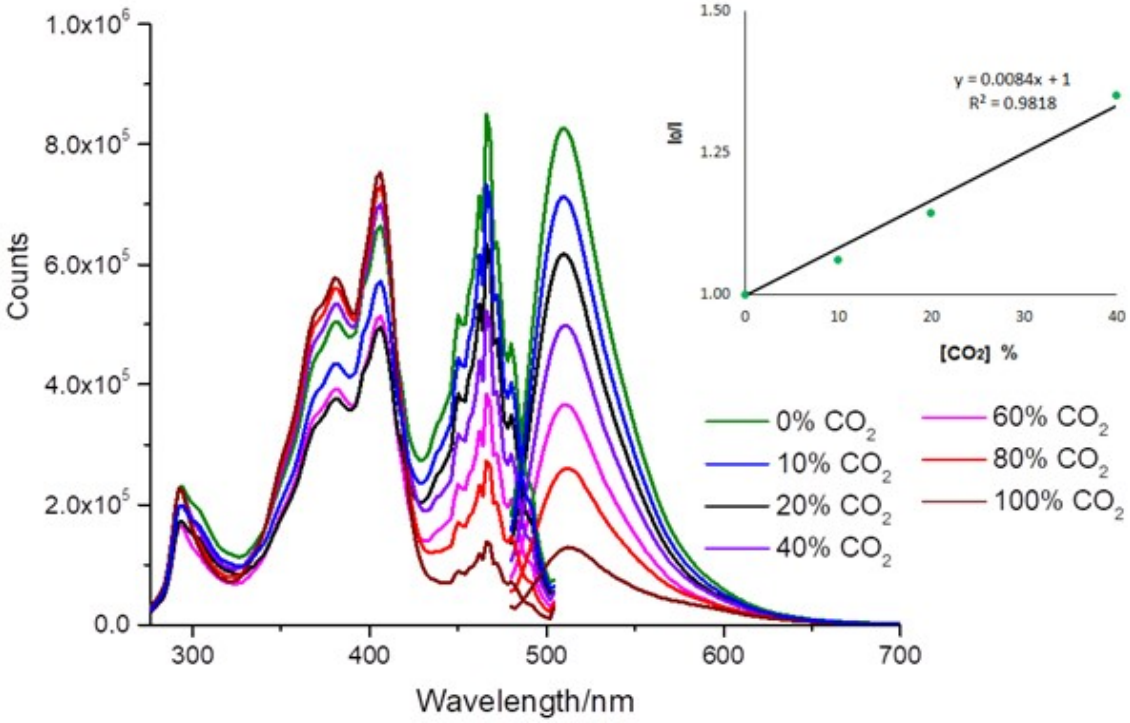

Figure 3: Emission and excitation spectra of additive-free-HPTS upon to exposure 0.0%, 10.0%, 20.0%; 40.0%; 60.0%; 80.0%; 100.0% CO_2(g).

Figures 4 and 5 show the CO_2-induced spectral behavior of HPTS with ZCO-CS and ZCO-H additives embedded in PMMA thin film for the 0-100% [CO_2] concentration range, respectively. The insets of Figures 4 and 5 show the linear response for the 0-40% [CO_2] concentration range. When comparing the CO_2-induced response of the HPTS-based used composites, ZCO-H showed a superior linear response and a considerably higher slope than ZCO-CS, which can be characterized by the equation y = 0.0102x + 1 and R^2 value of 0.9951.

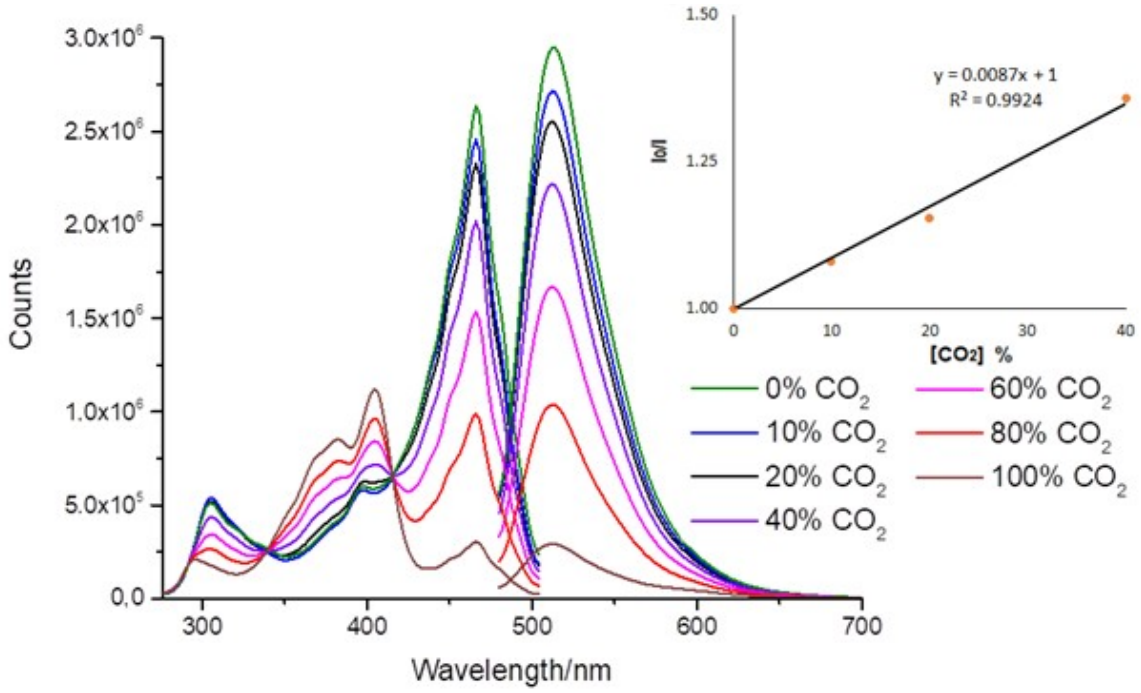

Figure 4: Emission and excitation spectra of HPTS as including ZCO-CS upon to exposure 0.0%, 10.0%, 20.0%; 40.0%; 60.0%; 80.0%; 100.0% CO_2(g).

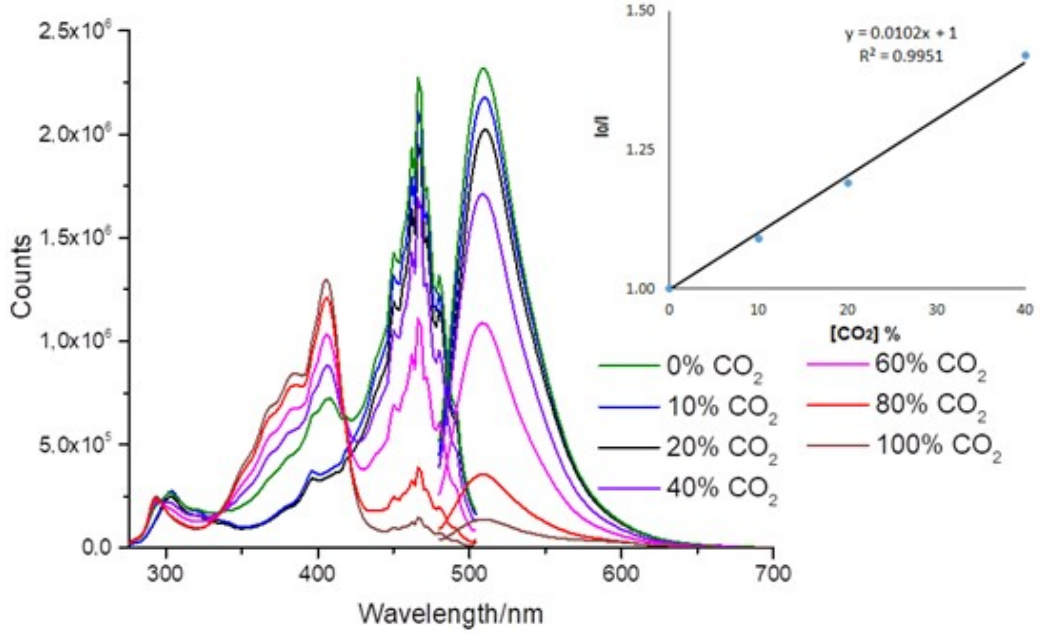

Figure 5: Emission and excitation spectra of HPTS as including ZCO-H upon to exposure 0.0%, 10.0%, 20.0%; 40.0%; 60.0%; 80.0%; 100.0% CO_2(g).

Figure 6 presents comparative calibration plots of composites used for the 0-100% [CO_2] concentration range. Comparing the CO_2-induced variations of the composites used, HPTS_ZCO-H exhibited a quite high slope between 0-100% pCO_2 and linear response for the 0-40% [CO_2] concentration range.

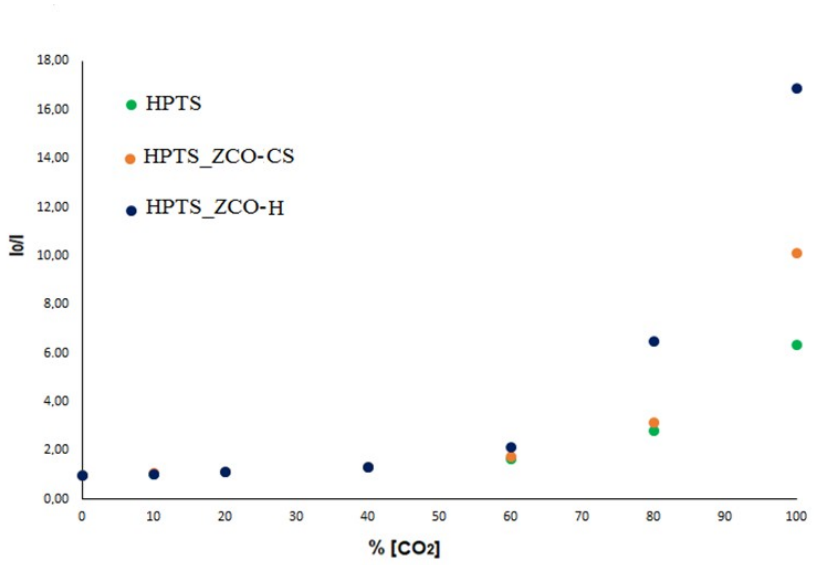

Figure 6: The CO_2-induced response of the additive-free HPTS and HPTS along with ZCO-H and ZCO-CS additives for the 0-100% [CO_2] range.

The use of additive metal oxide materials remarkably increased the CO_2-induced sensitivity of HPTS, enhancing the parameter of I_0/I_{100} from 6.36 of additive-free to 10.16, 16.90 for composites including, ZCO-CS, ZCO-H, respectively (See Table 4). The presence of too many free electrons on the surface of the semiconductor material allows a large number of oxygen species to be adsorbed by trapping the free electrons. Due to the presence of too many oxygen species on the ZnO/CuO structure surface, much more CO_2 gas reaches the surface, which leads to an increase in gas sensitivity. Apart from this, the presence of the ZnO/CuO heterostructure provides more reactive part and surface area, so it absorbs more CO_2 gas molecules (24).

Among the prepared HPTS-based sensing slides, the highest K_{SV} value of HPTS_ZCO-H underlines extreme sensitivity to CO_2, making ZnO/CuO proportion attractive for the detection of trace amounts of carbon dioxide. Wang et al. reported that sensitivity decreased in the case of reducing the Zn proportion in the structure (31). Lavin and co-workers also present that ZnO content in ZnO/CuO heterojunction enhances the photocatalytic efficiency of the structure (21). In our study, unlike the ZCO-CS, the Zn amount is higher for the ZCO-H heterostructure (confirmed by XPS). So the higher sensitivity of the ZCO-H structure along with HPTS dye can be attributed to the equilibrium of the interaction. When the CuO and ZnO materials are incorporated, electrons can be moved from n-type ZnO to p-type CuO until the system is equilibrated, which indicates the strong interaction between both materials.

This result indicates that HPTS dye with ZCO-H (K_{SV} = 1.02 × 10^{-2} $\%^{-1}$) has appropriated candidates for sensitive CO_2 sensing whereas the lower K_{SV} value of HPTS_ZCO-CS (K_{SV} = 8.7 × 10^{-3} $\%^{-1}$) (see Table 4).

Table 4: Photoluminescence-based properties and CO_2 sensitivity of HPTS dye in PMMA thin film with additives ZCO-CS and ZCO-H.

Cocktail name	Equation (Concentration range of 0–40 % [CO_2])	Ksv	Regression coefficient, R^2	I_0/I_{100}
Additive-free	y = 0.0084x + 1	8.4 × 10^{-3}	0.9818	6.36
ZCO-CS	y = 0.0087x + 1	8.7 × 10^{-3}	0.9924	10.16
ZCO-H	y = 0.0102x + 1	1.02 × 10^{-2}	0.9951	16.90

Decay Time Measurements

We measured and interpreted CO_2-induced decay time values of the HPTS dye including ZCO-H and ZCO-CS additives to clarify the CO_2 sensitivity upon excitation at 468 nm pulsed laser. The recorded decay time values were shown in Table 5. In addition, measuring the decay times of the thin films give us significant information for the interaction mechanism between fluorophore and quencher. The decay curves of the HPTS_ZCO-H and HPTS_ZCO-CS for 0-100% [CO_2] concentration were indicated in Figure 7. The decay time values of

HPTS_ZCO-H and HPTS_ZCO-CS decreased from 4.51 ns to 2.57 ns and from 4.52 ns to 3.89 ns when exposure to carbon dioxide, respectively.

Table 5: The decay time values of ZCO-H and ZCO-CS in the PMMA matrix.

Sample	To (0% CO_2)	Decay Time (ns)	Std. Dev. (ns)	Rel. (%)	To (100% CO_2)	Decay Time (ns)	Std. Dev. (ns)	Rel. (%)
HPTS_ZCO-H	τ_1	4.05	0.01	95.96	τ_1	0.42	0.01	34.96
	τ_2	15.45	0.06	4.04	τ_2	3.73	0.05	65.04
	τ_{avr}		**4.51 ns**		**τ_{avr}**		**2.57 ns**	
HPTS_ZCO-CS	τ_1	4.10	0.01	93.89	τ_1	0.75	0.02	21.04
	τ_2	11.04	0.02	6.11	τ_2	4.73	0.03	78.96
	τ_{avr}		**4.52 ns**		**τ_{avr}**		**3.89 ns**	

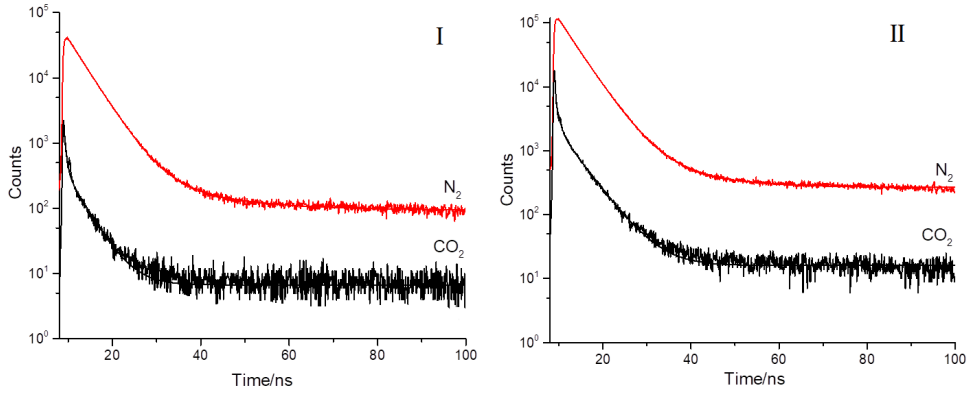

Figure 7: Decay curves of **I:** HPTS_ZCO-H **II:** HPTS_ZCO-CS.

The obtained results can be evaluated as electrical conductivity and charge mobility, resulting in a decrease in decay time values. In metal oxide semiconductors, the adsorbed or diffused gas reduces the carrier density and creates potential barriers between the oxide grains that cause a reduction in electrical conductivity. The same charge mobility that affects the conductivity also affects the luminescence and the decay time values decrease (35).

CONCLUSION

In this study, HPTS dye was used along with additives of ZnO/CuO heterostructures for the first time and thus HPTS dye has been shown to increase its sensitivity to CO_2 gas. The carbon dioxide sensitivities of the HPTS along with these additives are tuned via changing the proportion of ZnO and CuO. Although the I_0/I_{100} value of core-shell ZnO/CuO immobilized in PMMA thin film was 10.16, hybrid ZnO/CuO showed better sensitivity with the value of 16.90 upon to CO_2. The results show that the generation of heterojunction between ZnO and CuO in the synthesized ZnO/CuO structure makes free electrons, which facilitates the adsorption of CO_2 molecules on the surface and facilitates morphology and defects.

ACKNOWLEDGMENT

Characterization measurements were performed at Dokuz Eylul University, Center for Fabrication and Applications of Electronic Materials. I want to thank all.

CONFLICT OF INTEREST

The author declares that there are no conflicts of interest.

REFERENCES

1. Ali R, Saleh SM, Meier RJ, Azab HA, Abdelgawad II, Wolfbeis OS. Upconverting nanoparticle based optical sensor for carbon dioxide. Sensors and Actuators B: Chemical. 2010 Sep;150(1):126–31. <DOI>.

2. Chu C-S, Lo Y-L, Sung T-W. Review on recent developments of fluorescent oxygen and carbon dioxide optical fiber sensors. Photonic Sens. 2011 Sep;1(3):234–50. <DOI>.

3. Swickrath M, Anderson M, McMillin S, Broerman C. Application of Commercial Non-Dispersive Infrared Spectroscopy Sensors for Sub-ambient Carbon Dioxide Detection. In: 42nd International Conference on Environmental Systems [Internet]. San Diego, California: American Institute of

Aeronautics and Astronautics; 2012 [cited 2021 Aug 24]. <DOI>.

4. Shimizu Y, Yamashita N. Solid electrolyte CO2 sensor using NASICON and perovskite-type oxide electrode. Sensors and Actuators B: Chemical. 2000 Jun;64(1–3):102–6. <DOI>.

5. Malins C, MacCraith BD. Dye-doped organically modified silica glass for fluorescence based carbon dioxide gas detection. Analyst. 1998;123(11):2373–6. <DOI>.

6. Zeyrek Ongun M. Tuning CO2 sensitivity of HPTS by ZnO and ZnO@Ag nanoparticles. Journal of Photochemistry and Photobiology A: Chemistry. 2020 Sep;400:112664. <DOI>.

7. Neurauter G, Klimant I, Wolfbeis OS. Microsecond lifetime-based optical carbon dioxide sensor using luminescence resonance energy transfer. Analytica Chimica Acta. 1999 Feb;382(1–2):67–75. <DOI>.

8. Schutting S, Jokic T, Strobl M, Borisov SM, Beer D de, Klimant I. NIR optical carbon dioxide sensors based on highly photostable dihydroxy-aza-BODIPY dyes. J Mater Chem C. 2015;3(21):5474–83. <DOI>.

9. Schutting S, Borisov SM, Klimant I. Diketo-Pyrrolo-Pyrrole Dyes as New Colorimetric and Fluorescent pH Indicators for Optical Carbon Dioxide Sensors. Anal Chem. 2013 Mar 19;85(6):3271–9. <DOI>.

10. Borchert NB, Kerry JP, Papkovsky DB. A CO2 sensor based on Pt-porphyrin dye and FRET scheme for food packaging applications. Sensors and Actuators B: Chemical. 2013 Jan;176:157–65. <DOI>.

11. von Bültzingslöwen C, McEvoy AK, McDonagh C, MacCraith BD, Klimant I, Krause C, et al. Sol–gel based optical carbon dioxide sensor employing dual luminophore referencing for application in food packaging technology. Analyst. 2002;127(11):1478–83. <DOI>.

12. Nivens D. Multilayer sol–gel membranes for optical sensing applications: single layer pH and dual layer CO2 and NH3 sensors. Talanta. 2002 Sep 12;58(3):543–50. <DOI>.

13. Wolfbeis OS, Kovács B, Goswami K, Klainer SM. Fiber-optic fluorescence carbon dioxide sensor for environmental monitoring. Mikrochim Acta. 1998 Sep;129(3–4):181–8. <DOI>.

14. Neurauter G, Klimant I, Wolfbeis OS. Fiber-optic microsensor for high resolution pCO 2 sensing in marine environment. Fresenius' Journal of Analytical Chemistry. 2000 Mar 2;366(5):481–7. <DOI>.

15. Oter O, Polat B. Spectrofluorometric Determination of Carbon Dioxide Using 8-Hydroxypyrene-1,3,6-trisulfonic Acid in a Zeolite Composite. Analytical Letters. 2015 Feb 11;48(3):489–502. <DOI>.

16. McEvoy AK, Von Bueltzingsloewen C, McDonagh CM, MacCraith BD, Klimant I, Wolfbeis OS. Optical sensors for application in intelligent food-packaging technology. In: Glynn TJ, editor. Galway, Ireland; 2003 [cited 2021 Aug 24]. p. 806. <DOI>.

17. Ertekin K. Characterization of a reservoir-type capillary optical microsensor for pCO2 measurements. Talanta. 2003 Feb 6;59(2):261–7. <DOI>.

18. Oter O, Sabancı G, Ertekin K. Enhanced CO₂ Sensing with Ionic Liquid Modified Electrospun Nanofibers: Effect of Ionic Liquid Type. sen lett. 2013 Sep 1;11(9):1591–9. <DOI>.

19. Zeyrek Ongun M, Oğuzlar S, Köse Yaman P, Öter Ö. Tuning CO2 sensing properties of HPTS along with newly synthesized coordination polymers (CPs). Spectrochimica Acta Part A: Molecular and Biomolecular Spectroscopy. 2021 Dec;263:120224. <DOI>.

20. Arafat MM, Dinan B, Akbar SA, Haseeb ASMA. Gas Sensors Based on One Dimensional Nanostructured Metal-Oxides: A Review. Sensors. 2012 May 30;12(6):7207–58. <DOI>.

21. Lavín A, Sivasamy R, Mosquera E, Morel MJ. High proportion ZnO/CuO nanocomposites: Synthesis, structural and optical properties, and their photocatalytic behavior. Surfaces and Interfaces. 2019 Dec;17:100367. <DOI>.

22. Fan C, Sun F, Wang X, Majidi M, Huang Z, Kumar P, et al. Enhanced H2S gas sensing properties by the optimization of p-CuO/n-ZnO composite nanofibers. J Mater Sci. 2020 Jun;55(18):7702–14. <DOI>.

23. Zhyrovetsky VM, Popovych DI, Savka SS, Serednytski AS. Nanopowder Metal Oxide for Photoluminescent Gas Sensing. Nanoscale Res Lett. 2017 Dec;12(1):132. <DOI>.

24. Mariammal RN, Ramachandran K. Study on gas sensing mechanism in p-CuO/n-ZnO heterojunction sensor. Materials Research Bulletin. 2018 Apr;100:420–8. <DOI>.

25. Wang JX, Sun XW, Yang Y, Kyaw KKA, Huang XY, Yin JZ, et al. Free-standing ZnO–CuO composite nanowire array films and their gas sensing properties. Nanotechnology. 2011 Aug 12;22(32):325704. <DOI>.

26. Oter O, Ertekin K, Derinkuyu S. Ratiometric sensing of CO2 in ionic liquid modified ethyl cellulose matrix. Talanta. 2008 Jul 30;76(3):557–63. <DOI>.

27. Yang C, Cao X, Wang S, Zhang L, Xiao F, Su X, et al. Complex-directed hybridization of CuO/ZnO nanostructures and their gas sensing and photocatalytic properties. Ceramics International. 2015 Jan;41(1):1749–56. <DOI>.

28. Mahajan P, Singh A, Arya S. Improved performance of solution processed organic solar cells with an additive layer of sol-gel synthesized ZnO/CuO core/shell nanoparticles. Journal of Alloys and Compounds. 2020 Jan;814:152292. <DOI>.

29. Ongun MZ, Oter O, Sabancı G, Ertekin K, Celik E. Enhanced stability of ruthenium complex in ionic liquid doped electrospun fibers. Sensors and Actuators B: Chemical. 2013 Jul;183:11–9. <DOI>.

30. Chen W, Qiu Y, Zhong Y, Wong KS, Yang S. High-Efficiency Dye-Sensitized Solar Cells Based on the Composite Photoanodes of SnO 2 Nanoparticles/ZnO Nanotetrapods. J Phys Chem A. 2010 Mar 11;114(9):3127–38. <DOI>.

31. Wang X, Li S, Xie L, Li X, Lin D, Zhu Z. Low-temperature and highly sensitivity H2S gas sensor based on ZnO/CuO composite derived from bimetal metal-organic frameworks. Ceramics International. 2020 Jul;46(10):15858–66. <DOI>.

32. Choi MF. Spectroscopic behaviour of 8-hydroxy-1,3,6-pyrenetrisulphonate immobilized in ethyl cellulose. Journal of Photochemistry and Photobiology A: Chemistry. 1997 Apr;104(1–3):207–12. <DOI>.

33. Ratterman M, Shen L, Klotzkin D, Papautsky I. Carbon dioxide luminescent sensor based on a CMOS image array. Sensors and Actuators B: Chemical. 2014 Jul;198:1–6. <DOI>.

34. Dey A. Semiconductor metal oxide gas sensors: A review. Materials Science and Engineering: B. 2018 Mar;229:206–17. <DOI>.

35. Aydin I, Ertekin K, Demirci S, Gultekin S, Celik E. Sol-gel synthesized Sr4Al14O25:Eu2+/Dy3+ blue–green phosphorous as oxygen sensing materials. Optical Materials. 2016 Dec;62:285–96. <DOI>.